

---

Climate Change Initiative Extension (CCI+) Phase 2  
New Essential Climate Variables (NEW ECVs)  
High Resolution Land Cover ECV (HR\_LandCover\_cci)

---

End-to-End ECV Uncertainty Budget  
(E3UB)

---

Prepared by:

Università degli Studi di Trento  
Fondazione Bruno Kessler  
Università degli Studi di Pavia  
Università degli Studi di Genova  
Université Catholique de Louvain  
Politecnico di Milano  
LSCE  
CREAF  
University of Exeter  
e-GEOS s.p.a.  
Planetek Italia





UNIVERSITY  
OF TRENTO



UCLouvain  
Earth and Life Institute - Geomatics



	Ref	D2.3 – E3UB		
	Issue	Date	Page	
	1.1	14/01/2025	1	

## Changelog



Issue	Changes	Date
1.0	First issue	14/01/2025
1.1	Updated based on RIDs	14/02/2025

## Detailed Change Record

Issue	RID	Description of discrepancy	Sections	Change
1.0	ESA-01	How can be an AD the document itself? It should be Phase 1 E3UB v4.0	Applicable Documents / 1.3	This AD refers to E3UB from phase 1. The text is updated accordingly.
1.0	ESA-02	typo ATDB should be ATBD	Acronyms and abbreviations / 1.5	The typo is fixed.

## Contents

<b>1</b>	<b>Introduction.....</b>	<b>3</b>
1.1	Executive summary .....	3
1.2	Purpose and scope .....	3
1.3	Applicable documents.....	3
1.4	Reference documents .....	3
1.5	Acronyms and abbreviations.....	3
<b>2</b>	<b>SAR processing chain .....</b>	<b>4</b>
2.1	Input Data .....	5
2.2	Pre-Processing.....	5
2.3	Feature Extraction Uncertainties .....	6
2.4	Deep Learning Architecture and Training .....	6
2.5	Local Conditions .....	6
2.6	Validation and Ground Truth Data .....	7
<b>3</b>	<b>Decision Fusion .....</b>	<b>7</b>
3.1	Uncertainty in Hidden Markov Model .....	7
3.2	Uncertainty in Conditional Random Fields.....	7
3.3	Uncertainty Output .....	8
<b>4</b>	<b>References .....</b>	<b>9</b>

	Ref	D2.3 – E3UB		
	Issue	Date	Page	
	1.1	14/01/2025	3	

## 1 Introduction

### 1.1 Executive summary

This document provides an assessment of the end-to-end uncertainty budget the HRLC ECV products are associated with. HRLC products are based on a wide range of input data whose uncertainties propagate at different levels of dependency according to the data characteristics and the processing steps involved in the production. By taking into account the scarce availability of ground-measured reference information and the practical impossibility to collect physical measurements on wide areas as those selected for this project, the proposed uncertainty models will be, by necessity, theoretical.

Many steps of the processing chain (e.g., pre-processing, geolocation, classification, etc.) involve algorithms that come with uncertainty models associated to them. For instance, the classification task is able to output probabilistic posteriors that can be managed at the fusion level to infer uncertainty score pixel-wise. Both uncertainties of input data sets and processing model-related ones must be considered, including error propagation dynamics. The nature of the input data sets (discrete classes vs. continuous variables) and the associated error characteristics (random error/ bias, error distribution), including potential correlations between errors of different input variables should be evaluated. Finally, uncertainties related to the spatial scales of data sets, scaling issues related to the validation activity must be accounted for as well.

### 1.2 Purpose and scope

This document provides both a detailed overview of the main sources of uncertainty for each step of the full processing chain and representations of pixel-wise uncertainty for the final HRLC and LCC products.

This document deals with all known potential sources of error, uncertainty and known correlations in the data that are seen as potential contributors for the definition of an uncertainty product. The output for classification is given as a three layer data-structure that includes:

- Classification maps associated with both first- and second-best performers, in terms of posterior probability, as returned by the classification-fusion model.
- Actual values of posterior probabilities corresponding to the two above mentioned maps.
- Input quality index corresponding to the input optical-data quality, which is related to the number and temporal distribution of the images acquisitions used in the composite generation step.

The model uncertainty in Land Cover Change (LCC) reflects the propagation of uncertainties from earlier processing steps. The probability of change, representing the estimated occurrence probability of changepoints over time, serves as a key source of information for assessing the certainty of LCC products. Additionally, the availability of images on a yearly basis influences this uncertainty. When insufficient images are available for a given year, the change information is aggregated over a longer time span, resulting in increased uncertainty.

### 1.3 Applicable documents

**Ref. Title, Issue/Rev, Date, ID**

[AD1] CCI\_HRLC\_Ph1-D2.3\_E3UB, v4.0



[AD2] CCI\_HRLC\_Ph2-D2.2\_ATDB, latest version

### 1.4 Reference documents

**Ref. Title, Issue/Rev, Date, ID**

### 1.5 Acronyms and abbreviations

ATBD	Algorithm Theoretical Basis Document
DL	Deep Learning
E3UB	End-to-End ECV Uncertainty Budget
HR	High Resolution
LC	Land Cover
S1	Sentinel-1
SAR	Synthetic Aperture Radar

	Ref	D2.3 – E3UB		
	Issue	Date	Page	
	1.1	14/01/2025	4	

## 2 Optical processing chain

The Optical Processing Chain in Phase 2 builds upon the robust methodologies established in Phase 1 to deliver high-resolution, high-quality land cover products. This chain plays a critical role in processing Harmonized Landsat Sentinel-2 (HLS) data to ensure seamless integration of multi-sensor observations. The focus remains on harmonizing data from different platforms while accounting for uncertainties at each processing stage. By maintaining consistency with Phase 1, the updates introduced in Phase 2 improve usability and interpretability without altering the core uncertainty framework. The two primary components of the Optical Processing Chain are:

- Pre-Processing: Addressing sensor-specific corrections and harmonization to create composite datasets that form the basis for downstream analysis.
- Classification: Leveraging advanced machine learning and deep learning techniques to provide robust, pixelwise land cover maps with quantified uncertainties.

These components, in tandem, ensure the production of reliable land cover products while explicitly propagating and quantifying uncertainties from input data through to final outputs.

### 2.1 Optical pre-processing

The pre-processing stage is dedicated to preparing the optical data for classification. The data used in Phase 2 have been already processed for radiometric correction, cloud and shadow masking, and spectral harmonization. Phase 2 further process these data for composite generation. Each step incorporates well-established methodologies to minimize and quantify uncertainties [1]:

- Radiometric Correction: Radiometric correction is critical for standardizing reflectance values across different sensors (Landsat and Sentinel-2). Using the LaSRC algorithm, corrections consider atmospheric properties like aerosol optical thickness, column water vapor, and ozone levels. This ensures consistent surface reflectance values, with uncertainties quantified using in situ comparisons. Reflectance uncertainty varies between 0.11% and 1.4%, depending on the spectral band.
- Cloud and Cloud-Shadow Detection: Probabilistic approaches are used to mask clouds and their shadows. Each pixel is assigned a likelihood of being affected by cloud contamination, minimizing misclassifications. While physical measurements for validation are impractical, posterior evaluations rely on synthetic and observational benchmarks, allowing for refined accuracy metrics.
- Spectral Harmonization: HLS data processing requires addressing differences in spectral responses and solar-view geometries between Landsat and Sentinel-2. This step employs BRDF models to normalize illumination and observation conditions, particularly in areas with strong seasonal or angular variability. While this normalization enhances data consistency, residual uncertainties remain tied to the limitations of BRDF modeling.
- Composite Generation: Composite datasets are created by synthesizing multi-temporal observations into a single representative mosaic (representing a single month, a season, or a whole year). This process ensures consistent spatial and temporal coverage, weighted by the Input Quality Index (IQIX). The IQIX is strictly related to the number of composites in a given year that are generated with at least three valid acquisitions (i.e., non saturated, cloud and shadow free pixels). In the case of annual composites, the input quality is proportional to the number of valid acquisitions of the only composite.



### 2.2 Optical classification

The classification stage in Phase 2 introduces deep learning (DL) models for robust feature extraction and land cover mapping. This step generates full posterior probability distributions for all thematic classes, enabling a comprehensive understanding of classification uncertainty. Advanced DL architectures (e.g., Temporal CNNs, Swin-Transformers, Transformer Encoder) are utilized to model complex relationships within the HLS data. These models effectively handle diverse land cover scenarios, providing detailed classification outputs at high spatial resolution.

We can model the posterior probabilities using  $m$  linear classifiers on top of the extracted deep features. Each linear classifier implements a hyperplane that separates its corresponding class from the other classes. The equation of each hyperplane is

$$f_j(\mathbf{x}) = \mathbf{w}_j \cdot \mathbf{x} + b_j$$

where  $\mathbf{w}_j$  is a weight vector and  $b_j$  is a bias term. Each class-specific posterior probability is typically computed using the softmax function:

	Ref	D2.3 – E3UB		
	Issue	Date	Page	
	1.1	14/01/2025	5	

$$P(\hat{\ell}_i | \mathbf{x}_n; \boldsymbol{\vartheta}_i) = \frac{\exp(f_i(\mathbf{x}_n))}{\sum_{k=1}^m \exp(f_k(\mathbf{x}_n))}$$

Hence, the parameter set  $\boldsymbol{\vartheta}_i = (\mathbf{w}_i, b_i)$ . For any probabilistic-based classifier, plugging the posterior probabilities into the cross-entropy function and solving the equation (gradient methods) is at the core of the well-known learning rules and or backpropagation algorithms. Pixelwise uncertainty can be derived directly from the posterior probabilities, highlighting regions of low classification confidence. In particular, areas with overlapping class probabilities are identified as high-uncertainty zones, providing critical input for subsequent decision fusion processes. Classification uncertainties are influenced by the quality and representativeness of training datasets. Underrepresented land cover types, such as forested wetlands and shrublands, and inconsistencies in temporal coverage contribute to model uncertainties. These are mitigated through techniques like data augmentation, cross-validation, and balanced sampling.

The outputs of the optical classification module are designed to seamlessly integrate into downstream decision fusion steps. Key deliverables include:

- **Full Posterior Probability Distributions:** These provide a pixelwise representation of classification confidence across all thematic classes.
- **Input Quality Index:** Reflecting the reliability of the input HLS data, the IQIX supports the interpretation of classification results.

### 3 SAR processing chain

High-Resolution (HR) Land Cover (LC) maps, derived from the processing of Sentinel-1 (S1) Synthetic Aperture Radar (SAR) time series using deep learning (DL) architectures such as Swin-Unet, provide critical insights for environmental monitoring across large areas. However, various sources of uncertainty can degrade the quality and reliability of these maps.

The land cover classification pipeline based on SAR data relies on a multi-stage processing chain to generate high-resolution (10m) maps. This process includes pre-processing, feature extraction, classification, and post-processing steps, which introduce specific sources of uncertainty at each stage. Details from the Algorithm Theoretical Basis Document (ATBD) [AD2] have been incorporated to enrich the understanding of these uncertainties.

Identifying and mitigating sources of uncertainty is crucial for improving the accuracy and reliability of land cover maps derived from SAR data using DL networks.

This paragraph explores these uncertainties in the context of high-resolution land cover mapping, focusing on the key stages of the classification process and their impacts on the final outputs. However, all those aspects concerning potential sources of uncertainty which are common to the Phase 1 processing chain are already documented in the End-to-End ECV Uncertainty Budget (E3UB) deliverable [AD1] and will be included only in summary here.

#### 3.1 Input Data



The accuracy of land cover maps is directly influenced by the quality of the input SAR data. Several factors can introduce errors into the SAR data, affecting the final classification:

- **Noise and Artefacts:** The inherent noise in SAR data, such as speckle noise, can significantly reduce the clarity of the images and make it more difficult to distinguish between different land cover types.
- **Temporal Resolution and Coverage Gaps:** Inconsistent temporal coverage or insufficient data over specific time periods can cause gaps in the data, leading to a loss of continuity and making it difficult to track seasonal changes in land cover.

#### 3.2 Pre-Processing

The pre-processing steps, including radiometric calibration, geometric correction, and filtering, introduce potential sources of uncertainty:

- **Radiometric Calibration:** Inaccuracies during calibration may result in variations in pixel intensity values, impacting the classification of land cover types.
- **Geometric Correction:** The process of aligning SAR images to a common coordinate system can lead to distortions, especially in areas with significant terrain relief.
- **Speckle Noise Filtering:** While speckle noise can be reduced through advanced filtering techniques, the chosen method must balance noise suppression with the preservation of important image features. Over-filtering may result in a loss of critical information.

	Ref	D2.3 – E3UB		
	Issue	Date	Page	
	1.1	14/01/2025	6	

Errors in these steps, such as improper noise removal or inaccuracies in terrain correction, can propagate into the final land cover maps. The inherent speckle noise in SAR data adds to the complexity, with advanced filters like multitemporal despeckling providing significant improvements but also introducing potential loss of critical texture information.

### 3.3 Feature Extraction Uncertainties

Feature extraction relies on techniques such as mean, median, and max-min filtering, which aim to enhance relevant details while suppressing noise. However, the balance between noise reduction and feature preservation is critical. Additionally, seasonal compositing used to generate 'super-images' may fail to adequately capture dynamic or abrupt changes, particularly in regions with strong seasonal variability like Amazonia or Siberia.

### 3.4 Deep Learning Architecture and Training



DL models, such as Swin-UNet, are transformative tools in remote sensing applications like land cover classification. However, their performance is influenced by uncertainties arising from the quality and diversity of training data, hyperparameter optimization, and model generalization. The following paragraphs elaborate on these issues.

- **Imbalanced Training Datasets** The lack of adequate representation for all land cover types in the training dataset may skew the learning process. For instance, underrepresented classes such as forested wetlands in the Amazon region may lead to systematic misclassification all over the world in similar ecoregions. Addressing this issue requires balancing datasets through data augmentation or targeted sampling techniques [2].
- **Inconsistent Spatio-Temporal Coverage:** Temporal dynamics, such as seasonal floodings in Amazonia or vegetation cycles in Siberia, necessitate diverse temporal snapshots for robust training. Insufficient data coverage may result in poor model adaptation to temporal variations [3].
- **Overfitting and Underfitting:** Overfitting occurs when the model learns noise or minor details specific to the training data, limiting its generalization ability. Conversely, underfitting results stem from insufficient model complexity or inadequate training, and may miss critical patterns for classification [4].
- **Hyperparameter Selection:** Parameters such as the learning rate and dropout rate need fine-tuning to achieve an optimal balance between model complexity and data representation. Automatic optimization techniques, including Bayesian optimization or grid search, can assist in this process [5].
- **Diverse Land Cover Types:** Complex regions like the mixed land cover of African savannas or urban-rural interfaces are a tough challenge for model generalizability. Utilizing multi-sensor data or region-specific pretraining may enhance the model adaptability.
- **Climatic and Environmental Variability:** Extreme conditions, such as frozen landscapes in Siberia or dense tropical canopies in the Amazon region, introduce variability that standard models may not capture well.

### 3.5 Local Conditions

Regions such as Amazonia, Africa, and Siberia introduce unique challenges. Seasonal floodings in the Amazon region, sparse vegetation in African savannas, and extreme climatic conditions in Siberia are examples of situation that impact data quality and model performance, significantly contributing to uncertainties:

- **Amazonia:** The seasonal variations in vegetation and flooding patterns may introduce challenges in accurately identifying land cover types. Additionally, cloud cover is a common issue in tropical regions, which may interfere to the following Sar + optical data fusion or multi-sensor classification approaches.
- **Africa:** Sparse vegetation and diverse land cover types, such as savannas, forests, and agricultural areas, can create ambiguities in classification. The low resolution of some of the available SAR data may also limit the model's ability to distinguish between fine-scale land cover types
- **Siberia:** Extreme climatic conditions and frozen landscapes add another layer of complexity, especially when it comes to identifying land cover changes in snow-covered or permafrost regions. SAR data's sensitivity to moisture and surface roughness can make it difficult to discern between different types of land cover in these environments.

	Ref	D2.3 – E3UB		
	Issue	Date	Page	
	1.1	14/01/2025	7	

### 3.6 Validation and Ground Truth Data

The accuracy of the final land cover maps depends heavily on the availability and quality of ground truth data. Several challenges affect this validation process:

- **Limited Availability of Ground Truth Data:** In remote or inaccessible regions such as Siberia or large parts of Africa, ground truth data may be sparse or entirely unavailable, making it difficult to assess the accuracy of the classification results.
- **Spatial and Temporal Mismatches:** Ground truth data may not always align spatially or temporally with SAR data sets, leading to errors in classification accuracy during model validation.
- **Labelling Errors:** Errors in the manual or automated labelling of training or validation datasets may introduce bias, leading to misclassification or inaccurate assessment of land cover types.

## 4 Decision Fusion

The Decision Fusion processing chain in Phase 2 receives the classification results from both the optical and SAR processing chains along with their uncertainties, which are expressed by the pixel-wise posterior probabilities. The multi-sensor pixel-wise fusion process in Phase 2 uses the same approach as Phase 1 i.e., the logarithmic opinion pool (LOGP) which calculates the fused probability distribution that directly indicates the pixel-wise measure of uncertainty after the fusion (refer to Phase 1 E3UB v4.0 [AD1] for more detailed information). On the contrary, the subsequent multi-temporal fusion and spatial fusion steps are modified and improved in Phase 2 taking into account this uncertainty. In both cases, the improved formulations are probabilistic and Bayesian, a methodological approach that makes it possible to endow the resulting mapping product with an accompanying pixelwise posteriors, which takes into account the related spatial and temporal models.

The following subsections discuss the uncertainty related to the improvement of the multi-temporal model by the Hidden Markov Model (HMM) and spatial fusion model by the Conditional Random Field (CRF).

### 4.1 Uncertainty in Hidden Markov Model

The Hidden Markov Model (HMM) is a probabilistic-based model to consider the information from the whole time series, improving the cascade model which only takes into account the information of a pair of time steps. Given the joint fused posterior probability on each pixel,  $P_F(\boldsymbol{\ell}|\mathbf{x}) = P_F(\ell_1, \ell_2, \dots, \ell_T | \mathbf{x}_1, \mathbf{x}_2, \dots, \mathbf{x}_T)$  of the vector of all labels  $\boldsymbol{\ell} = (\ell_1, \ell_2, \dots, \ell_T)$ , where  $\mathbf{x} = (\mathbf{x}_1, \mathbf{x}_2, \dots, \mathbf{x}_T)$  refers to the collection of feature vectors of all time steps. A first-order HMM follows these two conditions:

$$P(\ell_t | \ell_{t-1}, \ell_{t-2}, \dots, \ell_1) = P(\ell_t | \ell_{t-1}) \quad \forall t \in \{2, 3, \dots, T\}$$



$$P(\mathbf{x} | \boldsymbol{\ell}) = \prod_t P(\mathbf{x}_t | \ell_t)$$

where the first condition ensures the Markovianity of the labels along the time, and the second one assumes the conditional independence on the relationship between observations and labels. Under these constraints, the posterior distribution  $P(\ell_t | \mathbf{x})$  of the label  $\ell_t$  at each time given all observations in the time series can be computed in closed form through a sequential iterative algorithm (forward-backward algorithm). This multitemporal pixelwise distribution simultaneously determines the output predicted land cover label and encodes the associated uncertainty. This process intrinsically expresses uncertainty in the form of probabilities. Indeed, it is worth emphasizing that, as compared to the fused pixelwise posterior obtained separately by LOGP on each date,  $P(\ell_t | \mathbf{x})$  takes explicitly into account the whole time series associated with the pixel in the modelling of uncertainty as well.

### 4.2 Uncertainty in Conditional Random Fields

Conditional Random Fields (CRFs) are a family of probabilistic graphical models allowing the inclusion of contextual information by considering the interactions between neighbouring pixels. Correspondingly, the uncertainty associated with the predicted class labels can also be computed from the energy function of the CRF model. The energy function of the CRF model that considers up to non-zero pairwise clique potentials can be written as:



	Ref	D2.3 – E3UB		
	Issue	Date	Page	
	1.1	14/01/2025	8	

$$U(\mathbf{L}|\mathbf{X}) = - \sum_{s \in S} \alpha \log P_F(\ell_s | \mathbf{x}_s) - \sum_{\substack{s \in S \\ r \in \partial s}} V_{sr}(\ell_s, \ell_r | \mathbf{X}),$$

where  $\mathbf{L}$  indicates the predicted label map and  $\mathbf{X}$  refers to the input image data.  $S$  is the pixel lattice,  $s$  is a notation for a generic pixel location  $(i, k)$ , and  $\partial s \subset S$  is the set of the corresponding neighbouring pixels.  $P_F(\ell_s | \mathbf{x}_s)$  specifies the fused posterior probability of label  $\ell_s$  (obtained through LOGP, as mentioned before),  $\alpha$  is a positive weight, and  $V_{sr}(\ell_s, \ell_r | \mathbf{X})$  defines the pairwise potential function, which is defined in detail in ATBD(Phase 2) v1.1 and combines a spatial Potts regularization with a contrast function based on the pixelwise posteriors.

The uncertainty in CRF can be estimated using a softmax function based on its local posterior energy:

$$\tilde{P}_{CRF}(\ell_s | \mathbf{x}_s, \{\ell_r\}_{r \in \partial s}) = \frac{\exp[-U(\ell_s | \mathbf{x}_s, \{\ell_r\}_{r \in \partial s})]}{\sum_{\omega_k} \exp[-U(\ell_s = \omega_k | \mathbf{x}_s, \{\ell_r\}_{r \in \partial s})]}$$

where  $\omega_k$  indicates  $k$ -th class,  $k = 1, 2, \dots, \mathcal{C}$ , where  $\mathcal{C}$  is the number of classes.  $U(\ell_s | \mathbf{x}_s, \{\ell_r\}_{r \in \partial s})$  expresses the local posterior energy function, which additively collects the energy contributions associated with pixel  $s$  in relation to its pixelwise fused posterior (unary term) and its spatial context (pairwise potential). Weights exist in the energy function, such as  $\alpha$  and other weight parameters inside the pairwise potential function  $V_{sr}(\cdot)$ . Such weights also generally affect the resulting uncertainty estimate  $\tilde{P}_{CRF}(\cdot)$ . For this reason, an additional parameterization on the uncertainty estimation is used, similar to what was done in Phase 1, by introducing a further tuneable parameter  $\mu$  so that the output of the uncertainty reflects the spatial structure of the CRF output. The value of  $\mu$  is determined experimentally to match the distribution of the posterior values after the fusion, so that the resulting product correctly propagate the uncertainty measures received from the optical and SAR processing chains. Hence the output CRF uncertainty is defined as:

$$\tilde{P}_{CRF}(\ell_s | \mathbf{x}_s, \{\ell_r\}_{r \in \partial s}) = \frac{\exp[-\mu U(\ell_s | \mathbf{x}_s, \{\ell_r\}_{r \in \partial s})]}{\sum_{\omega_k} \exp[-\mu U(\ell_s = \omega_k | \mathbf{x}_s, \{\ell_r\}_{r \in \partial s})]}$$



### 4.3 Uncertainty Output

In Phase 1, taking into account storage constraints and readability for climate users and a possibly broader public, the final output of uncertainty did not contain the complete set of the posterior probabilities of all  $\mathcal{C}$  classes – which is reasonable even in general terms, because the least probable classes may be associated with probability values close to zero. On the contrary, the largest posterior and the second largest posterior are stored. The former expresses the confidence of the selected land cover class, whereas the gap with respect the latter emphasizes an uncertainty margin. By default, we shall keep this formulation in Phase 2 as well, which makes the format output of uncertainty consist of:

- Classification maps containing the best and second-best thematic classes, that indicate the most probable class and the second most probable class on each individual pixel.
- Posterior probabilities that correspond to the best and second-best thematic classes.
- Input quality index corresponding to the optical input quality which is associated to the number and temporal distribution of the optical data acquisitions used in the composite generation step.

## 5 LandCover Change Detection

The final stage of the CCI HRLC processing chain, involving landcover change detection, is significantly influenced by uncertainties propagated from earlier steps, such as decision fusion, classification maps, and multisensor geolocation. These uncertainties also extend to abrupt change detection. DL models for feature extraction and land cover change detection introduced in Phase 2 (where advanced DL architectures, such as 3D CNNs, Swin-Transformers) are used to model complex relationships in multi-temporal multispectral data. These models provide posterior probabilities for land cover change detection, effectively capturing diverse land cover transitions and delivering detailed change detection outputs where a break point detector is employed. The break point detector decomposes time series data into trend ( $Tt$ ), seasonal ( $St$ ) and noise ( $et$ ) components,

	Ref	D2.3 – E3UB		
	Issue	Date	Page	
	1.1	14/01/2025	9	

identifying breakpoints that denote potential changes, along with their associated confidence intervals. The general model for decomposition is in the form of:

$$Y_t = Tt + St + et \quad (t = 1, 2, \dots, n)$$

In which  $Y_t$  is the observed data at time  $t$ . The method outputs breakpoints and confidence intervals for changes in the trend component. The magnitude and direction of changes, derived from the slope of consecutive linear models, help distinguish real abrupt changes from signal noise. By iteratively adjusting confidence levels, a probability for the change date is derived, indicating the uncertainty of the detected changes.

Another factor reported as the uncertainty of the detected changes is the reliability of the change. When sufficient data is available, changes are reported for consecutive years. If data is insufficient, the algorithm searches for reliable acquisitions within a six-year span, reporting the change year along with a reliability value indicating the temporal distance between the years used for change detection. This reliability value serves as an uncertainty measure for the reported change year

## 6 References

- [1] M. Claverie *et al.*, "The Harmonized Landsat and Sentinel-2 surface reflectance data set," *Remote Sensing of Environment*, vol. 219, pp. 145–161, Dec. 2018, doi: 10.1016/j.rse.2018.09.002.
- [2] X. X. Zhu *et al.*, "Deep Learning in Remote Sensing: A Comprehensive Review and List of Resources," *IEEE Geoscience and Remote Sensing Magazine*, vol. 5, no. 4, pp. 8–36, Dec. 2017, doi: 10.1109/MGRS.2017.2762307.
- [3] X. Zhang *et al.*, "Remote Sensing Object Detection Meets Deep Learning: A metareview of challenges and advances," *IEEE Geoscience and Remote Sensing Magazine*, vol. 11, no. 4, pp. 8–44, Dec. 2023, doi: 10.1109/MGRS.2023.3312347.
- [4] L. Zhang, L. Zhang, and B. Du, "Deep Learning for Remote Sensing Data: A Technical Tutorial on the State of the Art," *IEEE Geoscience and Remote Sensing Magazine*, vol. 4, no. 2, pp. 22–40, Jun. 2016, doi: 10.1109/MGRS.2016.2540798.
- [5] A. Ben Hamida, A. Benoit, P. Lambert, and C. Ben Amar, "3-D Deep Learning Approach for Remote Sensing Image Classification," *IEEE Transactions on Geoscience and Remote Sensing*, vol. 56, no. 8, pp. 4420–4434, Aug. 2018, doi: 10.1109/TGRS.2018.2818945.